Capillary instability, squeezing, and shearing in head-on microfluidic devices

Lingling Shui,[a] Albert van den Berg, and Jan C. T. Eijkel
BIOS/Lab-on-a-Chip Group, MESA+ Institute for Nanotechnology, University of Twente, 7500AE Enschede, The Netherlands

(Received 17 September 2009; accepted 2 November 2009; published online 17 December 2009)

We investigate two-phase (oil and water) flow in head-on microfluidic devices, which consist of two identical channels as inlets and the "long leg" as a constriction channel leading to a wider outlet section. Over an exceptionally broad range of flow rates of 10^{-4}–10 μl/min in 10–100 μm (hydraulic diameter) microchannels, corresponding to capillary numbers of 10^{-6}–10^{-1}, a two-phase flow map is presented. A rich flow behavior was found. The flow patterns observed were dripping, jetting, and threading. These phenomena are interpreted as caused by capillary instability, squeezing, and shearing by considering the contribution of different forces acting at the oil/water interface. This device provides us with a broad choice to generate droplets of different sizes and frequencies by modifying either the geometrical design or the flow rates. © *2009 American Institute of Physics*. [doi:10.1063/1.3268364]

I. INTRODUCTION

Multiphase microfluidics is a rapidly expanding field due to its great range of applications.[1] Complex fluidic systems play a very important role in pharmaceuticals, cosmetic, food, and oil industries. The fluids of interest in chemistry and biotechnology are rarely simple single-phase liquids.[2] Most of fluid transport, compartmental chemistry, interfacial phenomena, and applications employ multiphase fluidic systems. Both droplet-based flow and stratified flow have found applications for chemical and biological purposes.[3,4] Droplet-based flow is mainly used to create microcapsules, microreactors, micromixers, and bioassays. Stratified flow is applied in microreaction, extraction and separation, and kinetic studies.

The dynamics of the inner liquid threads is dominated by the pressure difference (normal stress) exerted across the interface.[5] Since interfacial tension acts only at interfaces, and viscous forces act in the bulk of fluids, boundary conditions must be considered. The normal force is defined as outward facing and a minus sign is due to pressure being defined as positive if it is compressive (i.e., inward facing). The boundary condition given balances normal forces at an interface

$$-P+\tau_v=\tau_\sigma+P_{\mathrm{hyd}}, \tag{1}$$

where P (Pa) is the local pressure, τ_σ (Pa) is the force per unit area due to interfacial tension, τ_v (Pa) is the viscous stress per unit area due to the fluidic dynamics, and P_{hyd} (Pa) is the hydrostatic pressure difference. We see that the interfacial force, dynamic force, and hydrostatic pressure difference all contribute to the force at the interface. The local force at the interface will be related to the typical fluid dimension (d) and flow speed (v), due to the dependence of the forces on them. The relative magnitude of the forces acting at the interface as a function of d and v is expressed in the dimensionless numbers shown in Table I.

The Bond number (Bo) is irrelative to flow speed, and only determined by the typical dimension d. At the microscale, $d<3$ mm, the gravity is negligible because of the small Bond number.[6,7] The capillary number (Ca) is the most often mentioned dimensionless number when describing multiphase flow at the nano- and microscale, especially for droplet-based flow.[3] Ca is independent of d; however, it is proportional to v. In microfluidic systems, the flow speed is commonly low, which makes interfacial tension dominant in most cases. In the experiments described in this paper, however, also higher flow speeds are applied. The balance between viscous and interfacial forces therefore changes considerably since Ca varies between 10^{-6} and 10^{-1}. The ratio of inertial effects to viscous forces is described by the Reynolds number (Re). Viscous flow is as a rule sustained for micro- and nanofluidics, and this holds as well for the experimental conditions reported in this paper.[3] The Weber number (We) is a function of both v and d. It can become dominant when high density fluids flow fast in microsystems.[8,9] In the experiments reported in this paper, We is smaller than 10^{-5}, implying that inertial effects are negligible.

Generally, in literature, flow rates in a range corresponding to $\mathrm{Ca}\in(10^{-3},10^{-1})$ have been investigated,[5,10,11] in which the droplet breakup mechanism is controlled by the

TABLE I. Dimensionless numbers relative to fluidic flow. Bo, Ca, We, and Re represent the Bond number, capillary number, Weber number, and Reynolds number, respectively. In the table, ρ is the fluid density, g is the gravity acceleration, σ means the interfacial tension, v indicates the flow speed, η is the dynamic viscosity, and d denotes a typical radial dimension. All forces are expressed per unit area.

	Gravity force	Viscous force	Inertial effect
Interfacial tension	$\mathrm{Bo}=\rho g d^2/\sigma$	$\mathrm{Ca}=\eta v/\sigma$	$\mathrm{We}=\rho v^2 d/\sigma$
Viscous force	Bo/Ca	1	$\mathrm{Re}=\rho v d/\eta$

[a]Electronic mail: l.shui@ewi.utwente.nl.

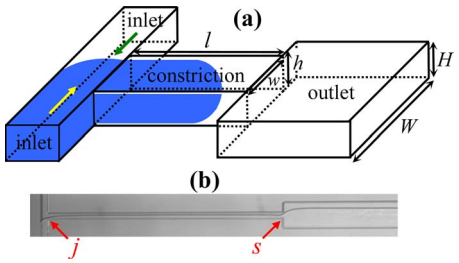

FIG. 1. (Color online) Microchannel configuration: (a) schematic three-dimensional drawing of the head-on devices, w—constriction channel width (10, 20, 30, 40, 60, 80, or 100 μm), l—constriction channel length (100, 500, or 1000 μm), h—constriction channel height (10 μm), W—outlet channel width (100 μm), and H—outlet channel height (10 μm); and (b) a photograph of threading oil-water two-phase flow. j and s indicate junction and step areas, respectively.

capillary number.[12,13] The mostly used geometries for two-phase flow are T-junctions,[10,13–15] flow-focusing devices (FFDs),[5,11,16–19] or coflowing devices.[9,20] Experiments have mostly been performed in microchannels fabricated in polydimethylsiloxane (PDMS) . As a consequence water-in-oil flow was obtained due to the wettability of PDMS for oil, and the permeability and deformability of PDMS would prevent investigators from using extremely low or high flow rates (or pressure).

The device we present here differs from the devices reported in literature both in geometry and in material used. A head-on microfluidic device is used, as shown in Fig. 1, consisting of two identical inlets, a constriction channel and a wide outlet channel, and made from glass. Two liquid phases (water-outer liquid and oil-inner liquid) are introduced from two inlets, meet at the junction (or the entrance of the constriction channel), and then flow through the constriction channel and step out into the wide outlet channel. The junction region (j) and the step region (s) from narrow constriction to wide outlet channel are two important geometrical features, as shown in Fig. 1(b). The total pressure across the oil-water interface (P) [Eq. (1)] in the j and s areas will be called P_j and P_s. Furthermore, we fabricated these microchannels in Pyrex glass, a hard and strong sealed material. The fact that the chip material is nondeformable enables us to pump fluids at high flow rate (or pressure), and the fact that they are nonpermeable enables fluid flow at very low flow rates. Therefore, we could perform experiments in a wide range of flow rates (or pressures). Flow behaviors ranging from dripping, jetting, to threading were obtained in the flow rate range 10^{-4}–10 μl/min corresponding to Ca of 10^{-6}–10^{-1}. We interpret the occurrence of these regimes by considering the contribution of the different forces acting at the interface mentioned above.

II. EXPERIMENTAL

The head-on configuration employed is illustrated in Fig. 1 where H and W indicate the outlet channel height and width, and w, l, and h are the constriction channel width, length, and height, respectively. Microchannels were fabricated in Pyrex glass using standard photolithography processes.[21,22] The interconnection holes were opened from the backside of the wafers by using powder-blasting techniques. Two wafers were then thermally bonded. The resulting bonded wafers were finally diced into 10×20 mm^2 chips. The chips were fixed in a homemade chip holder and connected to syringes via capillary tubing [outer diameter (OD): 1/16 in. and inner diameter (ID): 50 μm] and Nanoport connectors including a filter (INACOM INSTRUMENTS BV, Upchurch Scientific, Holland). Connectors and chips were sonically cleaned in deionized (DI) water for 15 min before use. Flow was controlled using a dual syringe pump (Harvard PHD 22/2000, HUGO SACHS ELECTRONIK-HAVARD APPARATUS Gmbh). The flow was visualized using an inverted microscope (Leica DMIRM) equipped with a mercury lamp and a fluorescence filter (filter cube B3) and recorded by using charge-coupled-device (CCD) cameras (Orca ER or Phantom V). The experimental setup is shown in Fig. 2.

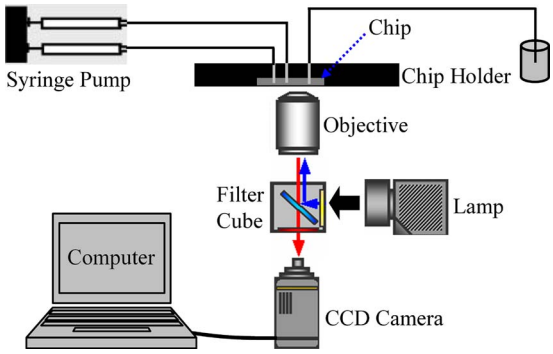

FIG. 2. (Color online) Schematic of the experimental setup.

The oil phase, which is hexadecane, shows up black in the images, and the water phase, which contains 0.01M sodium dodecyl sulfate [99+%, $CH_3(CH_2)_{11}OSO_3Na$] and 0.01M fluorescein sodium salt, appears white due to the excited fluorescein. All chemicals were bought from Sigma-Aldrich Chemie GmbH, Germany and used without further treatment. Droplet volume was calculated as measured droplet area from images multiplied by channel height when the droplet diameter was much bigger than the channel height, or calculated directly from the measured droplet diameter as a sphere when droplet size was comparable to channel height.

III. RESULTS AND DISCUSSION

The two immiscible phases (water and oil) fed from the two inlets by a syringe pump meet at the entrance of the constriction channel and generate oil-in-water flow due to the wettability of the channel walls. A typical flow map showing the different observed flow regimes based on the capillary numbers of oil (inner phase) and water (outer phase) phases (Ca_o and Ca_w) is displayed in Fig. 3. We distinguish five typical flow regimes, for which we use a nomenclature that is based on morphology and responsible mechanism: (I) geometry-determined dripping, (II) flow-rate-dependent dripping, (III) flow-rate-dependent jetting, (IV) geometry-determined jetting, and (V) threading. This complicated flow behavior as we will show is caused by the existence of the junction (j) and step (s) geometrical features. All regimes are illustrated by photomicrographs in Fig. 3(b).

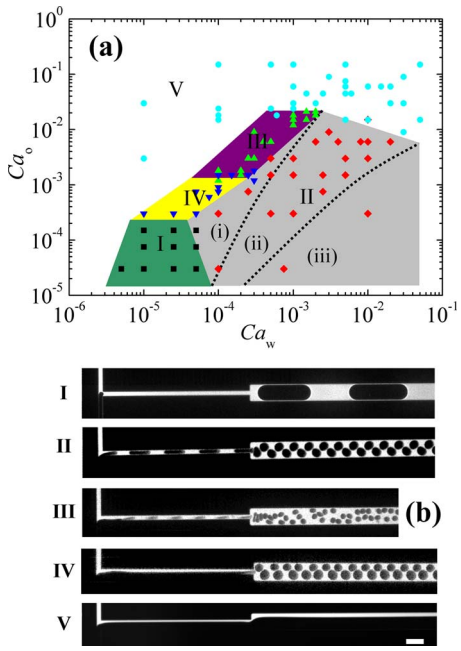

FIG. 3. (Color online) Flow map: (a) typical morphologically different flow regimes observed as a function of oil and water capillary numbers; (b) photographs of the corresponding flow patterns: (i) geometry-determined dripping (■), (II) flow-rate-dependent dripping (♦) [(i), (ii), and (iii): three subregimes treated in section (II)], (III) flow-rate-dependent jetting (▲), (IV) geometry-determined jetting (▼), and (v) threading (●). $h=10$ μm, $l=1000$ μm, and $w=30$ μm. The scale bar is 100 μm.

Morphologically we distinguish dripping, jetting, and threading. Dripping occurs when the oil thread on breakage occupies the entire constriction channel cross section downstream from the junction. Breakage thereby occurs at the junction. Jetting occurs when the oil thread only partly occupies the constriction channel. Breakage can thereby occur close to the junction or in the constriction channel downstream from the junction. Threading is distinguished from dripping and jetting, since the liquid threads display continuous morphology along both the constriction and the outlet channels.

As breakup mechanisms we distinguish capillary instability, squeezing, and shearing. Capillary instability is the breakup mechanism in geometry-determined dripping and jetting [(I) and (IV)], where the sudden expansion of the inner liquid (oil) at the step region leads to breakup at the junction (j) or the step (s) area to form droplets. Squeezing is the breakup mechanism in flow-rate-dependent dripping (II), which occurs when the oil thread blocks the constriction channel, and the subsequent buildup of the outer liquid pressure (water) leads to breakup at the junction (squeezing). Three subregimes, (i), (ii), and (iii), can be distinguished, as will be explained in section (II). The third mechanism, shearing, gives rise to the jetting (III) and threading regimes (V). Jetting (III) occurs when the outer liquid (water) shears the oil thread in the constriction channel, leading to breakup downstream from the junction. Threading (V) occurs at high shear conditions where viscous stress and interfacial tension are balanced. In the dripping and jetting flow regimes, after the generation of the first droplet, the oil phase flows as droplets and the water phase flows as segments between oil droplets and water films. The geometry-determined and flow-rate-dependent regimes correspond to a droplet formation, which is determined by the channel geometry and the flow rates of two phases, respectively.

A. Geometry-determined dripping caused by capillary instability (τ_σ driven breakup at the junction: j)

In our two-phase flow devices, at low flow rates, the hydrostatic pressure from the syringe pump pushes the oil phase slowly to advance into the constriction channel, and thus restricts the water flow to a thin film at the walls and a flow in the corners. An oil thread advances along the constriction channel toward the outlet channel; its tip is separated by a short water slug from the previous thread. The long oil thread in the constriction channel acts as a leaky piston, which is different from the situation in a circular capillary.[23,24] In a hydrophilic channel with a rectangular cross section, at small Ca, the oil phase is separated from the wall by a thin film and each corner by a meniscus, which has the same curvature as the cap.[23,25] The water phase can either bypass through the corners (corner flow) or drag the oil via the film (film flow).

The corner flow dominates at extremely low flow rates.[23–25] Figure 4(a) shows a typical droplet formation sequence in this flow regime. We plot the oil tip position (χ) in the constriction channel with respect to the junction versus time (t) at two different flow rates in Fig. 4(b) and the water segment length (l_w) versus time in the constriction channel in Fig. 4(c). The slopes of the rectangular and circular dotted lines in Fig. 4(b) are 3.65×10^{-4} and 7.06×10^{-4} m/s on average. The calculated oil flow velocities are 3.33×10^{-4} and 6.67×10^{-4} m/s when the oil flow rates (Q_o) are 2×10^{-3} and 4×10^{-3} μl/min, respectively. The measured flow velocities in the constriction channel are therefore approximately equal to the single pumping oil flow velocity. Since we kept the oil-to-water flow ratio constant most water must flow through the corners without shearing the oil in the constriction channel (significant shearing would cause breakup in the junction area). Furthermore, it can be seen from Fig. 4(c) that the water segment length increases with time, implying that the water is transported faster by the corner flow than the oil thread due to the cross-sectional shape.[25,26] The corner flow must therefore predominantly transport water in this region, and the water pressure work is dissipated predominantly by the friction in the corners.

Furthermore, in the regime of low Ca, the influence of the viscous pressure drop on breakage can be neglected. This can be verified explicitly by comparing the calculated hydrodynamic pressure $\tau_v[O(10^{-2}$ Pa)] at a flow rate of 10^{-4}–10^{-3} μl/min to the characteristic Laplace pressure $\tau_\sigma[O(10^4$ Pa)] in the system. Hence, under these conditions, the quasistatic oil-water interface has to obey the constraint of constant mean curvature along the entire oil thread. The interfacial force is therefore approximately equal to the hydrostatic pressure difference across the interface, and the total pressure across the oil-water interface is zero along the entire oil thread. However, as the oil thread front reaches the end of the constriction channel, the oil thread heads from the

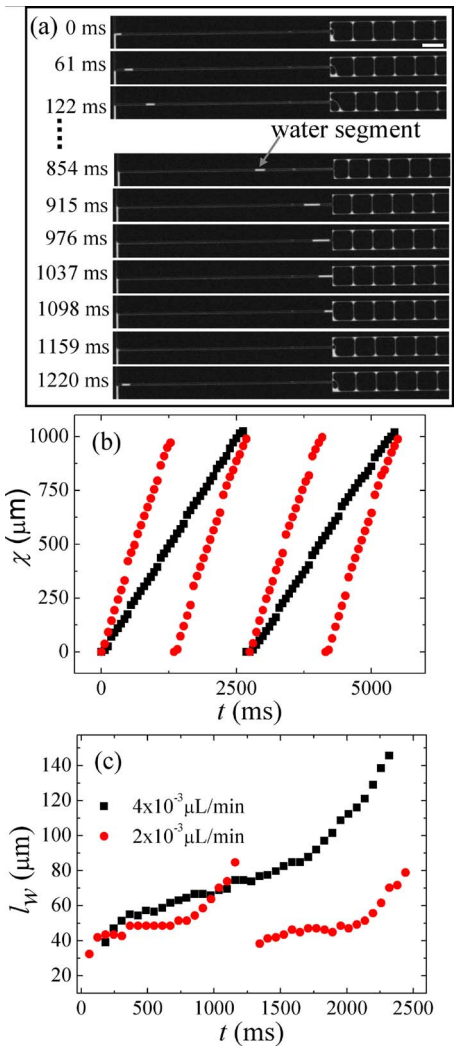

FIG. 4. (Color online) (a) Sequential snapshots of a cycle of droplet formation (oil appears as black and water as white) at $Q_o=Q_w=4\times10^{-3}$ μl/min, $l=1000$ μm, and $w=h=10$ μm; (b) the plot of the oil tip position with respect to junction vs time at two different oil flow rates: (■) 2×10^{-3} and (●) 4×10^{-3} μl/min; and (c) the plot of the water segment length vs time at two different oil flow rates: (■) 2×10^{-3} and (●) 4×10^{-3} μl/min. The water segment length is considered to be zero when it reaches the wide outlet channel.

shallow constriction channel into the wide outlet channel. The sudden change in channel width from w to W results in a sudden decrease in τ_σ. As a result, the oil tip expands, sucking the oil flow from the constriction into the outlet channel. The resulting increased oil flow rate will cause the oil thread at the junction to shrink. The increase in the interfacial curvature (force) at the junction finally leads to breakup of the oil thread at the junction to form a droplet. (Note that the two liquids therefore flow in parallel along the constriction channel. This would be considered as threading flow if there were no step in the design.[8]) After breakup the disconnected droplets flow downstream, while the oil thread retracts into the oil phase inlet channel. The process subsequently restarts. The breakup time is negligible compared to the long spreading time. The droplet volume is therefore approximately equal to the volume of the constriction channels.

The experimental results for the droplet volume coincide well with the theoretical values calculated from the constriction channel volume (Table II). The slight deviation for the small constriction channel may be due to the calculating method since the droplets were not fully disklike in the outlet channel. It turns out that the final droplet volume is, in fact, given almost exactly by the volume of the constriction channel provided that the latter is sufficiently long.[21]

TABLE II. Comparison of the constriction channel volume with the measured droplet volume in the geometry-determined dripping regime.

Constriction channel volume (nl)	Measured droplet volume (nl)[a]
0.08	0.0681
0.16	0.1611
0.32	0.3211
0.01	0.0104
0.10	0.0930

[a]Each measured droplet volume is obtained by averaging ten droplet volume.

B. Flow-rate-dependent dripping caused by squeezing (P_{hyd} driven breakup at junction)

As the water flow rate increases, the oil thread breaks in the junction before the emerging oil thread tip reaches the wide outlet channel. This occurs above a certain threshold flow rate. The droplet size decreases when the imposed water flow rate increases and the oil flow rate decreases in the same microfluidic device. We explain this droplet generation mechanism by "squeezing," as was prior described by Garstecki *et al.*[5,10] The droplet formation in this regime can be divided into five stages, as shown in Fig. 5: (a) The oil tip first intrudes at the junction, (b) the oil tip grows and blocks almost the entire cross section of the constriction channel, (c) the water squeezes the oil thread at the junction, (d) the oil thread starts to break at the junction, and (e) an oil droplet detaches from the oil thread, and the oil thread retracts.

The oil thread slowly blocks the cross section of the constriction channel after entering, and because the shear stresses exerted on the tip by the water phase are not strong

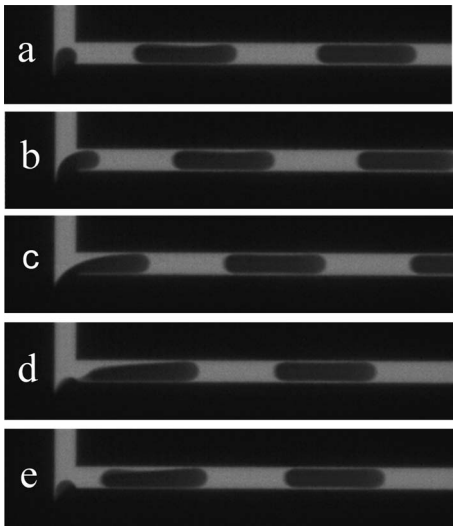

FIG. 5. Squeezing dynamics: time series of a cycle of droplet formation at the junction: (a) entering, (b) blocking, (c) squeezing, (d) breaking, and (e) detaching.

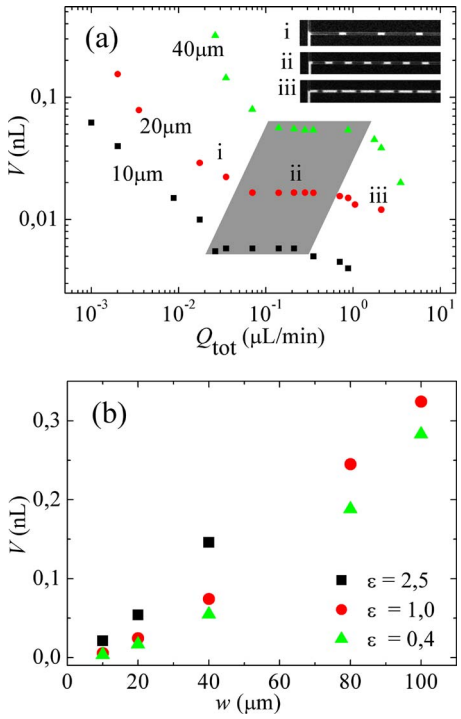

FIG. 6. (Color online) Flow-rate-dependent dripping: (a) droplet volume as a function of Q_{tot} in three different devices with $h=10$ μm, $l=400$ μm, and $w=10$, 20, and 40 μm at $\varepsilon=1$. The insets show different flow patterns observed in the three subregimes observed; (b) droplet volume as a function of constriction channel width at different flow rate ratios (ε) in subregime (ii).

enough to deform the tip, the water is confined to flow in the corners and in a film between the oil thread and the channel walls. The flow in the film leads to a buildup of pressure in water phase upstream of the tip. When the buildup pressure is larger than the pressure in the oil tip ($P_j<0$) the water starts to squeeze the neck of the oil thread. The squeezing then leads to the breakup of the oil tip and the detachment of a droplet from the oil thread.

The volume of a generated droplet (V) is now expected to be proportional to the breakup time (t_b) (the time interval during which the immiscible thread is open), multiplied by the inner liquid (oil) flow rate (Q_o) in the same device:[5,27] $V=Q_o t_b$. The experiments show that the water film thickness between the oil thread and the channel wall (λ) is negligible in comparison to the channel width in a range of intermediate flow rates. The cross-sectional area of oil and water phases is then constant in the same channel. The squeezing displacement speed of water to oil is thus proportional to the water flow rate (Q_w).[5,10,28] The breakup time $t_b \propto 1/Q_w$; thus at these flow rates $V=t_b Q_o \propto Q_o/Q_w$, the droplet volume is proportional to the oil-to-water flow rate ratio (ε). In our experiments the flow rate ratio was kept constant, and the squeezing mechanism would therefore lead to a constant droplet volume. We indeed observed such behavior over approximately one order of magnitude of flow rate [subregime (ii) in Fig. 6(a)]. This regime in which the droplet size is independent of flow rate at constant flow ratio is similar to previous reported regimes in T-junction and FFD devices.[5,10,28]

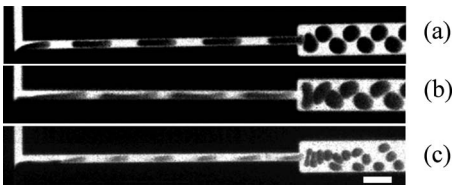

FIG. 7. Jetting induced by increasing flow speed: (a) $Q_o=0.1$ μl/min, $Q_w=0.05$ μl/min; (b) $Q_o=0.3$ μl/min, $Q_w=0.15$ μl/min; and (c) $Q_o=0.5$ μl/min, $Q_w=0.25$ μl/min. The scar bar is 100 μm.

When we looked at the detail of the plot [Fig. 6(a)] of the droplet volume as a function of total flow rate ($Q_{tot}=Q_o+Q_w$) at constant ε in this regime II, we found two flow ratio-dependent subregimes [(i) and (iii)] before and after that of subregime (ii), which as a function of the capillary numbers were also approximately indicated in Fig. 3(a). The reason for the existence of subregime (i) is not clear. The existence of subregime (iii) can be explained by the incipient shearing of water phase at higher flow rates.[29] In this regime, we observed that the oil thread only partially blocks the constriction channel. The breakup time t_b is therefore mainly determined by the time the oil tip travels from the inlet to the breakup point, which implies that t_b is a function of both Q_o and Q_w. Thus droplet volume V is not proportional to ε in this subregime (iii). Depending on the flow rate ratio, this small regime is relatively wide or narrow: wide at low ε and narrow at high ε.

At the same squeezing speed, t_b is proportional to the squeezing distance (the distance over which the oil thread has to be squeezed in order to break it, and hence it is equal to the oil thread diameter) $(w-2\lambda)$, which is $t_b \propto (w-2\lambda)$. We therefore also investigated the influence of geometry on droplet volume by varying the constriction channel width (w) from 10, 20, 40, 80, to 100 μm in regime (ii). The droplet volume as a function of constriction channel width is shown in Fig. 6(b), and it can be seen that the droplet volume increases with the constriction channel width.

C. Flow-rate-dependent jetting caused by shearing (τ_y driven breakup downstream from the junction)

As the capillary number is further increased, the oil thread breakup point moves progressively downstream, and a jet in the constriction channel is formed (as seen in Fig. 3). This transition experiences an intermediate regime as flow rate increases, where the growing droplets move downstream while still connected to the fluid in the tip through a fluid neck [Fig. 7(b)]. Finally, a clear jetting regime is obtained, where the oil thread does not break at the junction but at the tip away from the junction downstream in the constriction channel [Fig. 7(c)].

We follow the main line of the theoretical explanation for the transition due to the force the water phase exerts on the emerging oil thread. In the squeezing regime II, the oil thread blocks the constriction channel and the increasing water pressure subsequently breaks the oil thread. In the junction area, the interface, however, also experiences a viscous force stretching the oil thread downstream, decreasing the oil thread width, and preventing buildup of pressure in the water

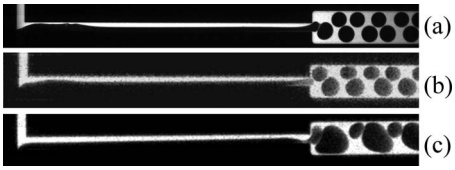

FIG. 8. [(a)–(c)] Geometry-determined capillary instability. The scale bar is 100 μm.

phase and hence squeezing. When the interfacial tension is balanced by viscous forces, the oil thread travels downstream until breakup occurs at its tip where the stress gradient across the jet relaxes. (Droplets do not form at the junction where $P_j \approx 0$ but form at the thread tip where the pressure at the oil thread tip $P_{\mathrm{tip}} < 0$.) The dripping to jetting transition can therefore be induced by increasing flow speed to increase the viscous forces;[14,20] see Fig. 7. The droplet size can be theoretically approximated by equating viscous stress and interfacial tension.[29]

D. Geometry-determined jetting caused by capillary instability (τ_σ driven breakup in the step area: *s*)

As mentioned above, the relaxation of stress gradient induces the breakup of the oil thread tip to droplets due to the interfacial instability. In the head-on microfluidic circuit, there is a geometrical step change (s) between the narrow constriction channel and the wide outlet channel. Fluid dynamics changes when water and oil flow together through this geometrical step change. At low oil and water flow rates (regime I) it was seen that the resulting drop in interfacial tension caused a breakup of the oil thread downstream at the junction area. At increasing oil flow rate, breakup instead was seen to occur at the step area. We explain this by the increased oil supply rate, preventing a sufficient pressure drop at the junction for breakup. Now the decreasing oil pressure on droplet expansion leads to a local thinning of the oil thread and breakage at the step area. In the head-on devices there therefore exists a specific geometry-determined capillary-instability regime (Fig. 8), which is different from other reported regimes.[8,9]

The flow in this capillary-instability regime is sensitive to changes in flow speed or geometry. Bifurcations in the droplet size were, for example, observed as shown in Figs. 8(a)–8(c). This sensitivity is understandable since the oil thread is not confined by the walls as in regime (I) and hence easily becomes unstable. This process could also be expressed in another way as breakup of an oil thread tip induced by a step change in geometry.[30]

E. Threading (τ_ν driven, no breakup)

Finally, a threading regime is observed where water and oil phases flow parallel to each other both in constriction and outlet channels. The inner more viscous oil liquid is focused and encapsulated by the water phase in the center of the constriction and outlet channels. This behavior is obtained by further increasing the water or oil flow rates to the point where the dynamic pressure difference overcomes both the interfacial forces and the geometrically induced pressure change. The viscous force of the water phase drags the interface straight downstream, and the pressure in the oil phase keeps the thread flow continuously. Therefore, no droplet formation was observed in the view field as defined before. The significant shape differences between the threads shown in Fig. 9 are due to the large flow speed difference between the oil and water phases in the different cases. The transition to this regime is not sudden but experiences an intermediate regime where the oil-water interface undulates but does not break. A smooth threading flow is sustained at higher flow rates.

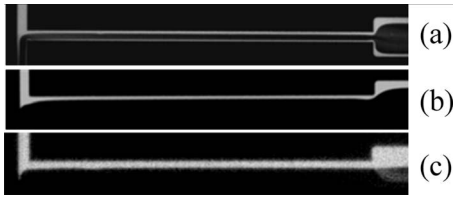

FIG. 9. Threading in head-on microfluidic channels. (a) $Q_w = 0.5Q_o = 0.5$ μl/min, (b) $Q_w = Q_o = 0.75$ μl/min, and (c) $Q_w = 2Q_o = 1$ μl/min.

IV. CONCLUSIONS AND OUTLOOK

Oil and water two-phase flow was investigated in glass head-on devices. A broad range of flow rates could be investigated due to the stable, hard, and impermeable wall material. A number of different flow regimes were observed, and a basic theoretical framework was provided to understand the different mechanisms of droplet formation by considering the different forces acting in the system. It was found that the rich flow behavior was caused by the specific channel layout chosen. This device therefore provides us with the choice to generate droplet-based flow in the regimes that are determined either by flow rate or device geometry.

ACKNOWLEDGMENTS

This research was supported by the Dutch Ministry of Economic Affairs through a Nanoimpuls grant. The authors gratefully acknowledge Professor G. M. Homsy and Sumita Pennathur for offering the use of the high speed camera and for helpful discussions.

[1] B. Zheng, J. D. Tice, L. S. Roach, and R. F. Ismagilov, Angew. Chem., Int. Ed. **43**, 2508 (2004).
[2] T. Pfohl, F. Mugele, R. Seemann, and S. Herminghaus, ChemPhysChem **4**, 1291 (2003).
[3] L. Shui, J. C. T. Eijkel, and A. van den Berg, Adv. Colloid Interface Sci. **133**, 35 (2007).
[4] A. Günther and K. F. Jensen, Lab Chip **6**, 1487 (2006).
[5] P. Garstecki, G. M. Whitesides, and H. A. Stone, Phys. Rev. Lett. **94**, 164501 (2005).
[6] H. A. Stone, A. D. Stroock, and A. Ajdari, Annu. Rev. Fluid Mech. **36**, 381 (2004).
[7] E. Berthier and D. J. Beebe, Lab Chip **7**, 1475 (2007).
[8] T. Cubaud and T. G. Mason, Phys. Fluids **20**, 053302 (2008).
[9] A. S. Utada, A. Fernandez-Nieves, H. A. Stone, and D. A. Weitz, Phys. Rev. Lett. **99**, 094502 (2007).
[10] P. Garstecki, M. J. Fuerstman, H. A. Stone, and G. M. Whitesides, Lab Chip **6**, 437 (2006).
[11] P. Garstecki, I. Gitlin, W. DiLuzio, G. M. Whitesides, E. Kumacheva, and H. A. Stone, Appl. Phys. Lett. **85**, 2649 (2004).

[12]B. Zheng, J. D. Tice, and R. F. Ismagilov, Anal. Chem. **76**, 4977 (2004).
[13]J. D. Tice, H. Song, A. D. Lyon, and R. F. Ismagilov, Langmuir **19**, 9127 (2003).
[14]J. D. Tice, A. D. Lyon, and R. F. Ismagilov, Anal. Chim. Acta **507**, 73 (2004).
[15]T. Thorsen, R. W. Roberts, F. H. Arnold, and S. R. Quake, Phys. Rev. Lett. **86**, 4163 (2001).
[16]R. Dreyfus, P. Tabeling, and H. Willaime, Phys. Rev. Lett. **90**, 144505 (2003).
[17]J. M. Gordillo, Z. D. Cheng, A. M. Ganan-Calvo, M. Marquez, and D. A. Weitz, Phys. Fluids **16**, 2828 (2004).
[18]S. L. Anna, N. Bontoux, and H. A. Stone, Appl. Phys. Lett. **82**, 364 (2003).
[19]P. Garstecki, M. J. Fuerstman, and G. M. Whitesides, Phys. Rev. Lett. **94**, 234502 (2005).
[20]A. M. Gañán-Calvo and P. Riesco-Chueca, J. Fluid Mech. **553**, 75 (2006).
[21]L. L. Shui, F. Mugele, A. van den Berg, and J. C. T. Eijkel, Appl. Phys. Lett. **93**, 153113 (2008).
[22]L. L. Shui, E. S. Kooij, D. Wijnperle, A. van den Berg, and J. C. T. Eijkel, Soft Matter **5**, 2708 (2009).
[23]H. Wong, C. J. Radke, and S. Morris, J. Fluid Mech. **292**, 95 (1995).
[24]H. Wong, C. J. Radke, and S. Morris, J. Fluid Mech. **292**, 71 (1995).
[25]A. Mazouchi and G. M. Homsy, Phys. Fluids **13**, 1594 (2001).
[26]E. Lajeunesse and G. M. Homsy, Phys. Fluids **15**, 308 (2003).
[27]B. J. Adzima and S. S. Velankar, J. Micromech. Microeng. **16**, 1504 (2006).
[28]J. H. Xu, G. S. Luo, S. W. Li, and G. G. Chen, Lab Chip **6**, 131 (2006).
[29]M. De Menech, P. Garstecki, F. Jousse, and H. A. Stone, J. Fluid Mech. **595**, 141 (2008).
[30]C. Priest, S. Herminghaus, and R. Seemann, Appl. Phys. Lett. **88**, 024106 (2006).